

**PREPUBLICACIONES DEL DEPARTAMENTO  
DE MATEMÁTICA APLICADA  
UNIVERSIDAD COMPLUTENSE DE MADRID  
MA-UCM 2013-04**

**Evaluation of the differences of process variables  
in vertical and horizontal configurations of  
High Pressure Thermal (HPT) processing systems  
through numerical modelling**

N. A. S. Smith, K. Knoerzer and A. M. Ramos

Marzo-2013

<http://www.mat.ucm.es/deptos/ma>  
e-mail:matemática\_aplicada@mat.ucm.es



# Evaluation of the differences of process variables in vertical and horizontal configurations of High Pressure Thermal (HPT) processing systems through numerical modelling

N. A. S. Smith<sup>a</sup>, K. Knoerzer<sup>b</sup>, Á. M. Ramos<sup>a,\*</sup>

<sup>a</sup>*Instituto de Matemática Interdisciplinar, Departamento de Matemática Aplicada, Facultad de Ciencias Matemáticas, Universidad Complutense de Madrid, Spain.*

<sup>b</sup>*The Commonwealth Scientific and Industrial Research Organisation (CSIRO), Division of Animal, Food and Health Sciences, Werribee, Victoria, Australia.*

---

## Abstract

High Pressure Thermal (HPT) processing of foods is a preservation technology which satisfies consumer demand for high-quality products. Numerical modelling can be used to predict locally specified temperature profiles arising during HPT processing, which is very important in order to ensure microbiological food safety and quality. To date all of the models developed and published on prediction of temperature and flow distribution are based on, to the best of our knowledge, vertically oriented HPT units. However, because of the increase of horizontal units in industry, and the lack of published work on horizontal models, it was seen important to bridge this research gap in order to advance the technology further. In this work a horizontal model was developed by adapting a previously validated vertical one. It was shown that the temperature performance and uniformity is different for the two configurations, indicating that the research conducted on vertical systems is not directly transferable to horizontal systems in HPT processing.

### *Keywords:*

high pressure, horizontal system, vertical system, heat and mass transfer, modelling, simulation, temperature distribution, uniformity

---

\*Corresponding author

*Email addresses:* [nas.smith@mat.ucm.es](mailto:nas.smith@mat.ucm.es) (N. A. S. Smith),  
[kai.knoerzer@csiro.au](mailto:kai.knoerzer@csiro.au) (K. Knoerzer), [angel@mat.ucm.es](mailto:angel@mat.ucm.es) (Á. M. Ramos)

*Preprint submitted to Innovative Food Science and Emerging Technologies March 13, 2013*

---

## 1. Introduction

High Pressure Processing (HPP) of foods is a preservation technology increasing in popularity and number of industrial applications globally, as it satisfies consumer demand for high-quality products with minimal degradation of organoleptic and nutritional properties. In the past years, HPP has been used for pasteurisation of foods because it permits microbial and to some extent enzymatic inactivation without heating the product much beyond room temperature. In combination with elevated temperatures, HPP also has a potential for high-temperature short-time sterilisation of shelf-stable low-acid food products. It has become clear that HPP offers major advantages to the food preservation and processing industry.

In HPP an increase of temperature during the compression phase can be observed due to partial conversion of mechanical work into internal energy. Due to the differences of the thermo physical properties, different materials undergo different temperature changes, which can result in temperature gradients throughout the HPT processing chamber and the product, causing non-uniform temperature distributions during processing. Therefore, being able to simulate and optimise the spatially resolved temperature evolution during a High Pressure (HP) process is very important to be able to ensure microbiological food safety, and also food quality.

The fluid flow in HP systems also has a significant influence on the homogeneity of a pressurised product. The compression of a liquid system changes its thermo dynamic and fluid dynamic state, leading to a fluid flow governed by forced convection into the treatment chamber during compression. The increase in temperature induces heat exchange within the liquid and solid and also heat exchange with the walls of the pressure chamber. Consequently, density differences occur which lead to free convection of the fluid.

Several authors have done extensive research in developing models to predict transient temperature and flow distributions, uniformity, and the loss of compression heating through high pressure vessel walls during all HPP steps. In Denys et al. (2000a,b); Hartmann & Delgado (2002, 2003); Hartmann et al. (2003, 2004) the authors used discrete numerical modelling and computational fluid dynamics (CFD) to predict temperature and flow distribution inside the HP vessel. More recent models include solid materials Infante et al. (2009); Juliano et al. (2008); Knoerzer et al. (2007); Otero et al.

(2007). In Ghani & Farid (2007) the authors predict temperature and flow distribution of a HP process in a three-dimensional vessel, and in Juliano et al. (2008); Knoerzer et al. (2007) the flow and temperature fields inside a pilot-scale unit for HP sterilisation conditions are numerically predicted and experimentally validated. In most of these works, special attention has also been given to the distribution of enzyme and microbial inactivation throughout the chamber and packages, aiming to ensure uniformity.

To the best of our knowledge, all of the models developed and published to date on prediction of temperature and flow distribution of a HP process have one common feature: they are models based on vertically oriented HP units. This is because, as stated in Mujica-Paz et al. (2011), the original HPP equipment units were vertical. However, the current trend is to supply horizontal units at industrial scale. A horizontal orientation avoids sub-level construction requirements, eliminates height, and floor load restrictions, makes system installation easier, facilitates product flow in the plant and reduces the risk of confusing treated and unprocessed product Mujica-Paz et al. (2011).

Because of the increase of horizontal units in industry, and the lack of published work on horizontal models, it was seen important, if not essential, to bridge this research gap in order to be able to advance the technology further, particularly with respect to HPT, which, to date, has not yet been commercialised. Nowadays, most of the experimental data available from researchers is for HP processes which have taken place in a vertical unit, due to the fact that laboratory or pilot-scale units are mostly vertical. The experimental resources required to be able to setup a horizontal laboratory-scale unit to obtain experimental data was not an available option. Therefore, designing a horizontal model from scratch was not seen reasonable. Instead, a horizontal model was developed by adapting an existing vertical one, which had previously been validated Infante et al. (2009); Otero et al. (2007). In this way, the differences between the vertical and horizontal models can be shown, stating the research need for developing horizontal models, which is essential for the industry.

It is clear that the major reason for the differences between vertical and horizontal models, even if they have exactly the same process conditions, is caused by the fluid flow pattern, and, therefore, differences in convective heat transfer. For upward flow in vertical tubes, the effect of free convection is to accelerate the fluid particles near the wall. This creates steeper velocity and temperature gradients near the wall, and hence higher heat transfer rates. To

satisfy continuity considerations, the increased velocity near the wall results in flow retardation at the tube centre and, in extreme cases, a reversal of flow at the tube centre may even occur (see, e.g., Kupper et al. (1969); Oliver (1962)). The flow pattern produced by free convection inside a horizontal tube is quite different to the vertical case; transverse fluid movement is more important. When a fluid in a horizontal tube is heated, the buoyancy forces cause movement of the fluid upwards at the sides and downwards at the centre. If combined with forced flow (which we do not consider in this work), this effect sets up forward moving spirals and the resulting flow pattern may not be entirely steady (see, e.g., Oliver (1962)).

Throughout this paper it will be shown that the horizontal and vertical flow inside a liquid-type food undergoing a HP process are indeed different, and therefore so is the temperature distribution, which could be problematic for the food manufacturing industry if uniformity of pursued effects such as enzymatic or microbial inactivation are required. In the following Sections the development of a heat transfer model to determine the temperature and flow distribution inside a sample treated with HP in a horizontally oriented vessel will be discussed, and the results compared to the ones obtained with the heat transfer model of a HP system placed vertically, with exactly the same process conditions.

## 2. The process models

The starting point of the model development is the model published in Infante et al. (2009), which is a vertical two-dimensional (2D) axis-symmetric model. The selection of an axis-symmetric model is very common in HPP modelling of vertically oriented devices, given that in many cases the system comprises axis-symmetric features, and has been successfully used and validated in several papers (see, e.g. Knoerzer & Chapman (2011); Knoerzer et al. (2010a); Knoerzer & Chapman (2011); Knoerzer et al. (2007); Otero et al. (2007)). The model derived in Infante et al. (2009) for liquid-type foods includes conduction and convection effects, and the flow is assumed to be laminar. Other more complex models, which also include turbulence effects (such as, e.g. Knoerzer et al. (2010a); Knoerzer & Chapman (2011); Knoerzer et al. (2007)), could have been chosen as the starting model. However, due to the complexity of solving a horizontal model, we decided to keep it as simple as possible.

For a horizontally oriented HP system, however, there are no longer only axis-symmetric features, and therefore a three-dimensional (3D) model is required. For this reason, both vertical and horizontal 3D models were developed, in order to compare them. In a first step, the 2D results of Infante et al. (2009) will be compared to the 3D vertical model for validation purposes and to check the efficiency of the 3D model solver used. In a subsequent step, the 3D horizontal and the 3D vertical models will be compared, and the differences of the results shown.

## 2.1. Geometries

### 2.1.1. Vertically oriented geometries

Following Infante et al. (2009), for a sample of liquid-type food, the computational vertical 2D axis-symmetric geometry considered is given in Figure 1, with the following sub-domains:

- $\Omega_F$ : domain that contains the food sample.
- $\Omega_C$ : cap of the sample holder (typically rubber).
- $\Omega_P$ : domain occupied by the pressurising medium.
- $\Omega_S$ : domain of the steel that surrounds the rest of the domains.

The boundary of  $\Omega$  (defined as  $\overline{\Omega} = \overline{\Omega_F \cup \Omega_C \cup \Omega_P \cup \Omega_S}$ ) is denoted by  $\Gamma$ , where we can distinguish:

- $\Gamma_r \subset \{L\} \times [0, H]$ , where the temperature is known (reference temperature).
- $\Gamma_{up} = [0, L] \times \{H\}$ , where heat transfer with the environment may take place.
- $\Gamma \setminus \{\Gamma_r \cup \Gamma_{up}\}$ , that has zero heat flux either by axial symmetry or by isolation of the equipment.

Star notation ( $[ ]^*$ ) was used to denote the 3D domains generated by rotating all the domains explained above along the axis of symmetry ( $\{0\} \times (0, H)$ ). The resulting 3D vertical geometry is depicted in Figure 2b. In Section 4.1 it will be shown that the solution given by the axis-symmetric 2D vertical model is almost identical to the 3D model.

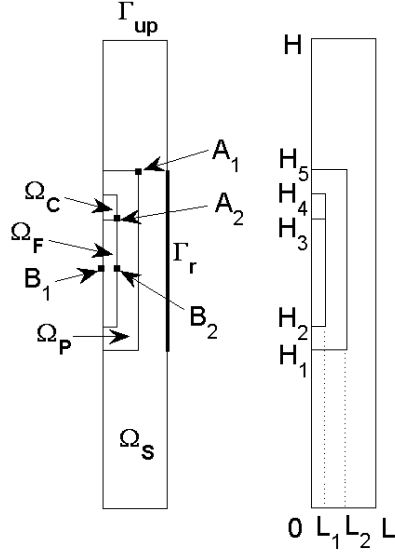


Figure 1: 2D axis-symmetric computational domain

### 2.1.2. Horizontally oriented geometry

Because in the horizontal case there are no longer only axis-symmetric features, the model cannot be reduced to a 2D model. However, there is a computational simplification that can be made: the model can be solved in only half a cylinder (cutting it longitudinally), thereby reducing the number of degrees of freedom. The resulting “half” 3D horizontal geometry is depicted in Figure 2c.

### 2.2. Heat and mass transfer model

When applying HP to food, the variations of temperature due to the compression/expansion that takes place in both the food sample and the pressurising medium have to be taken into account. Also, during and after the compression, there is heat exchange between the pressure chamber, the pressurising medium and the food sample. Hence, the distribution of temperatures will be transient. Furthermore, in the fluid medium (the pressurising fluid and the food sample when it is in liquid state) temperature variations imply fluid density variation, leading to free convection during the

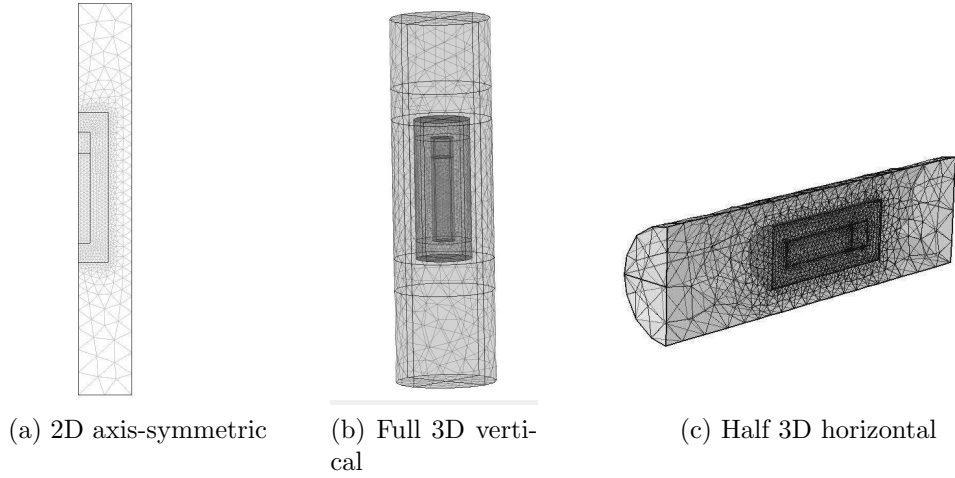


Figure 2: Computational configurations

high pressure process. Therefore, conduction and convection are considered in the model, taking into account heat and mass transfer.

In Infante et al. (2009), two significant cases were distinguished: solid- and liquid-type foods. For the purposes of this work, only liquid-type foods are considered, because due to convection effects inside the food sample, the differences between the vertical and horizontally oriented chambers will be more pronounced than when only considered conduction effects inside the food sample, which is the case for solid-type foods. Hence, following Infante et al. (2009), the model for a liquid-type food was considered, which includes heat transfer by conduction and convection. The convection occurs in both the food sample and the pressurising medium regions,  $\Omega_F$  and  $\Omega_P$ , in which two different velocity fields are considered,  $\mathbf{u}_F$  and  $\mathbf{u}_P$ , respectively. The pressurising medium and the food are separated by the sample holder and do not mix. It is assumed that the pressurising fluid is compressible and Newtonian. Assuming that the food is also a compressible Newtonian fluid,

the governing equations are

$$\left\{ \begin{array}{l} \rho C_p \frac{\partial T}{\partial t} - \nabla \cdot (k \nabla T) + \rho C_p \mathbf{u} \cdot \nabla T = \alpha \frac{dP}{dt} T \quad \text{in } \Omega^* \times (0, t_f), \\ \rho \frac{\partial \mathbf{u}_F}{\partial t} - \nabla \cdot \eta (\nabla \mathbf{u}_F + \nabla \mathbf{u}_F^t) + \rho (\mathbf{u}_F \cdot \nabla) \mathbf{u}_F \\ \quad = -\nabla p - \frac{2}{3} \nabla (\eta \nabla \cdot \mathbf{u}_F) + \rho \mathbf{g} \quad \text{in } \Omega_F^* \times (0, t_f), \\ \rho \frac{\partial \mathbf{u}_P}{\partial t} - \nabla \cdot \eta (\nabla \mathbf{u}_P + \nabla \mathbf{u}_P^t) + \rho (\mathbf{u}_P \cdot \nabla) \mathbf{u}_P \\ \quad = -\nabla p - \frac{2}{3} \nabla (\eta \nabla \cdot \mathbf{u}_P) + \rho \mathbf{g} \quad \text{in } \Omega_P^* \times (0, t_f), \\ \frac{\partial \rho}{\partial t} + \nabla \cdot (\rho \mathbf{u}_F) = 0 \quad \text{in } \Omega_F^* \times (0, t_f), \\ \frac{\partial \rho}{\partial t} + \nabla \cdot (\rho \mathbf{u}_P) = 0 \quad \text{in } \Omega_P^* \times (0, t_f), \end{array} \right. \quad (1)$$

where  $\rho$  is the density ( $\text{kg m}^{-3}$ ),  $C_p$  the specific heat capacity ( $\text{J kg}^{-1} \text{K}^{-1}$ ),  $k$  the thermal conductivity ( $\text{W m}^{-1} \text{K}^{-1}$ ),  $\mathbf{g}$  is the gravity constant vector ( $\text{m s}^{-2}$ ),  $\eta$  is the dynamic viscosity ( $\text{Pa s}$ ),  $p = p(x, t)$  is the pressure generated by the mass transfer inside the fluid,  $P + p$  is the total pressure ( $\text{Pa}$ ) in the pressurising medium ( $\Omega_F^*$ ) and  $t_f$  is the final time ( $\text{s}$ ). The right hand side of the first equation of (1) is the heat generation due to the change of pressure  $P = P(t)$  ( $\text{Pa}$ ) and therefore compression applied by the equipment (chosen by the user within the machine limitations) and  $\alpha$  ( $\text{K}^{-1}$ ) is the thermal expansion coefficient, that is given by

$$\alpha = \begin{cases} \alpha_F, & \text{thermal expansion coefficient of the food in } \Omega_F^*, \\ \alpha_P, & \text{thermal expansion coefficient of the pressurising fluid in } \Omega_P^*, \\ 0, & \text{elsewhere.} \end{cases}$$

This term results from the following law (see Knoerzer et al. (2007))

$$\frac{\Delta T}{\Delta P} = \frac{\alpha T V}{M C_p} = \frac{\alpha T}{\rho C_p}, \quad (2)$$

where  $\Delta T$  denotes the temperature change due to the pressure change  $\Delta P$ ,  $V$  is the volume and  $M$  the mass.

System (1) has to be completed with appropriate point, boundary and initial conditions depending on the HP machine. In this work the same conditions as in Otero et al. (2007) were used for a pilot unit (ACB GEC Alsthom, Nantes, France) located at the Instituto del Frio, CSIC, Spain

$$\left\{ \begin{array}{ll} k \frac{\partial T}{\partial \mathbf{n}} = 0 & \text{on } (\Gamma^* \setminus (\Gamma_r^* \cup \Gamma_{\text{up}}^*)) \times (0, t_f), \\ k \frac{\partial T}{\partial z} = h(T_{\text{env}} - T) & \text{on } \Gamma_{\text{up}}^* \times (0, t_f), \\ T = T_r & \text{on } \Gamma_r^* \times (0, t_f), \\ \mathbf{u}_F = 0 & \text{on } \Gamma_F^* \times (0, t_f), \\ \mathbf{u}_P = 0 & \text{on } \Gamma_P^* \times (0, t_f), \\ T(0) = T_0 & \text{in } \Omega^*, \\ \mathbf{u}_F(0) = 0 & \text{in } \Omega_F^*, \\ \mathbf{u}_P(0) = 0 & \text{in } \Omega_P^*, \\ p = 10^5 & \text{on } \mathbf{A}_1 \times (0, t_f), \\ p = 10^5 & \text{on } \mathbf{A}_2 \times (0, t_f), \end{array} \right. \quad (3)$$

where  $\mathbf{n}$  is the outward unit normal vector on the boundary of the domain,  $T_0$  (K) is the initial temperature,  $T_r$  (K) is the reference temperature on  $\Gamma_r^*$ ,  $T_{\text{env}}$  (K) is the environment temperature (constant) and  $h$  ( $\text{W m}^{-2} \text{K}^{-1}$ ) is the heat transfer coefficient;  $\Gamma_F^*$  denotes the boundary of  $\Omega_F^*$ ,  $\Gamma_P^*$  denotes the boundary of  $\Omega_P^*$  and  $\mathbf{A}_1$ ,  $\mathbf{A}_2$  are points of  $\Gamma_P^*$  and  $\Gamma_F^*$ , respectively (see Figure 1).

### 2.3. Simplified model with constant thermo physical properties

In Infante et al. (2009) system (1)-(3) was solved by using a 2D axis-symmetric version of it. In this work, also the full 3D model is solved, to then compare the results to the 2D axis-symmetric model. Because of the difficulty of solving a 3D model, it was decided to follow one of the simplified models proposed in Infante et al. (2009). Namely, a simplified model based on the Boussinesq approximation (which is denoted by LB in Infante et al. (2009)). Material properties  $C_p$ ,  $k$ ,  $\alpha$  and  $\eta$  are considered to be constant (instead of temperature and pressure dependent), and are set to their mean

value ( $\bar{C}_p$ ,  $\bar{k}$ ,  $\bar{\alpha}$  and  $\bar{\eta}$ , respectively) in the range of temperature and pressure considered in the process;  $\rho$  is also chosen as a constant value  $\bar{\rho}$ , except for the gravitational force  $\rho\mathbf{g}$  that appears in the second and third equations of system (1), where  $\rho$  remains dependent on temperature and pressure (in order to keep the effect of the gravitational forces). Furthermore, the food and pressurising fluids are assumed to be incompressible. This model is given by

$$\left\{ \begin{array}{ll} \bar{\rho}\bar{C}_p \frac{\partial T}{\partial t} - \bar{k}\nabla^2 T + \bar{\rho}\bar{C}_p \mathbf{u} \cdot \nabla T = \bar{\alpha} \frac{dP}{dt} T & \text{in } \Omega^* \times (0, t_f), \\ \bar{\rho} \frac{\partial \mathbf{u}_F}{\partial t} - \bar{\eta}\nabla^2 \mathbf{u}_F + \bar{\rho}(\mathbf{u}_F \cdot \nabla)\mathbf{u}_F = -\nabla p + \rho\mathbf{g} & \text{in } \Omega_F^* \times (0, t_f), \\ \bar{\rho} \frac{\partial \mathbf{u}_P}{\partial t} - \bar{\eta}\nabla^2 \mathbf{u}_P + \bar{\rho}(\mathbf{u}_P \cdot \nabla)\mathbf{u}_P = -\nabla p + \rho\mathbf{g} & \text{in } \Omega_P^* \times (0, t_f), \\ \nabla \cdot (\mathbf{u}_F) = 0 & \text{in } \Omega_F^* \times (0, t_f), \\ \nabla \cdot (\mathbf{u}_P) = 0 & \text{in } \Omega_P^* \times (0, t_f), \end{array} \right. \quad (4)$$

with boundary and initial conditions given by (3).

System (4) together with its boundary and initial conditions (3) are valid for all the proposed geometries in Section 2.1. For the 2D axis-symmetric model it may be rewritten in cylindrical coordinates (see Infante et al. (2009)). For the 3D horizontal “half” model, heat flux and flow symmetric boundary conditions have to be added to (3) at the “cutting” boundary.

When comparing this simplified model to the full one in Infante et al. (2009), it gave acceptable errors and was proven to be faster and easier to implement on the computer. Hence, the reason for using this simplification for the 3D model. The simplified 2D model was compared to the simplified 3D model. All following references to these models will be denoted 2D and 3D model.

#### 2.4. Comparing dimensionless convection effects for vertical and horizontal model

It was seen important to find a dimensionless quantity for convection effects for both the vertical and horizontal models, to evaluate their relevance. For this, the first equation of (4) is the starting point, i.e. the convective heat transfer equation

$$\bar{\rho}\bar{C}_p \frac{\partial T}{\partial t} - \bar{k}\nabla^2 T + \bar{\rho}\bar{C}_p \mathbf{u} \cdot \nabla T = \bar{\alpha} \frac{dP}{dt} T \quad (5)$$

where  $\bar{\rho}$ ,  $\bar{C}_p$ ,  $\bar{k}$ ,  $\bar{\alpha}$  are considered to be constant (they are set to their mean value in the temperature and pressure range).

Firstly, given that the pressure function in equation (5) only appears in a derivative form, and that the pressure applied on these processes is typically a piecewise linear function in time (hence such a derivative is usually piecewise constant) the pressure variable is not made dimensionless. Instead, the pressure derivative  $\frac{dP}{dt}(t)$  is rewritten as

$$\frac{dP}{dt}(t) = \begin{cases} \frac{\gamma}{t_p}, & 0 < t \leq t_p, \\ 0, & t > t_p, \end{cases} \quad (6)$$

where, for the sake of simplicity, it is assumed that  $\frac{dP}{dt}(t) = \frac{\gamma}{t_p} > 0$  ( $P$  linear) for all  $t \in [0, t_p]$ , and  $\gamma$  (Pa) is the maximum pressure reached (it is also assumed that atmospheric pressure is 0 MPa, instead of 0.1 MPa, which is typically the real value). After time  $t_p$  the pressure is maintained constant at the maximum value, and therefore the derivative is zero (other cases can be also studied similarly).

Equation (5) is made dimensionless by setting

$$\hat{x} = \frac{x}{L_r}, \quad \hat{y} = \frac{y}{L_r}, \quad \hat{z} = \frac{z}{L_z}, \quad \hat{t} = \frac{t}{\tau}, \quad \hat{T} = \frac{T}{\Theta}, \quad (\hat{u}_x, \hat{u}_y, \hat{u}_z) = \frac{1}{U}(u_x, u_y, u_z)$$

where  $\Theta$ ,  $U$ , and  $\tau$  are suitable temperature, velocity, and time scales, respectively.  $L_r$  is a radial length scale and  $L_z$  a vertical length scale.

Thus, equation (5) becomes

$$\begin{aligned} \frac{\bar{\rho}\bar{C}_p\Theta}{\tau} \frac{\partial \hat{T}}{\partial \hat{t}} - \bar{k}\Theta \left( \frac{1}{L_r^2} \left( \frac{\partial^2 \hat{T}}{\partial \hat{x}^2} + \frac{\partial^2 \hat{T}}{\partial \hat{y}^2} \right) + \frac{1}{L_z^2} \frac{\partial^2 \hat{T}}{\partial \hat{z}^2} \right) \\ + \bar{\rho}\bar{C}_p\Theta U (\hat{u}_x, \hat{u}_y, \hat{u}_z) \cdot \left( \frac{1}{L_r} \frac{\partial \hat{T}}{\partial \hat{x}}, \frac{1}{L_r} \frac{\partial \hat{T}}{\partial \hat{y}}, \frac{1}{L_z} \frac{\partial \hat{T}}{\partial \hat{z}} \right) = \frac{\alpha\gamma\Theta}{t_p} \hat{T}. \end{aligned} \quad (7)$$

Equation (7) is then divided by  $\bar{\rho}\bar{C}_p\Theta/\tau$ , resulting in

$$\begin{aligned} \frac{\partial \hat{T}}{\partial \hat{t}} - \frac{\bar{k}\tau}{\bar{\rho}\bar{C}_p} \left( \frac{1}{L_r^2} \left( \frac{\partial^2 \hat{T}}{\partial \hat{x}^2} + \frac{\partial^2 \hat{T}}{\partial \hat{y}^2} \right) + \frac{1}{L_z^2} \frac{\partial^2 \hat{T}}{\partial \hat{z}^2} \right) \\ + \tau U \left( \frac{\hat{u}_x}{L_r} \frac{\partial \hat{T}}{\partial \hat{x}} + \frac{\hat{u}_y}{L_r} \frac{\partial \hat{T}}{\partial \hat{y}} + \frac{\hat{u}_z}{L_z} \frac{\partial \hat{T}}{\partial \hat{z}} \right) = \frac{\alpha\gamma\tau}{\bar{\rho}\bar{C}_p t_p} \hat{T}. \end{aligned} \quad (8)$$

If the chamber is placed vertically (see Figure 1), the fluid in the vertical model is moving up and down the chamber, whilst in the horizontal case it will move from left to right. Therefore, it is assumed that the velocity in the vertical case is mainly moving in the vertical direction, i.e.  $u_z \gg u_x, u_y$  (or equivalently,  $\hat{u}_z \gg \hat{u}_x, \hat{u}_y$ ) whilst in the horizontal case it mainly moves in the radial direction, hence  $u_z \ll u_x, u_y$  (or equivalently,  $\hat{u}_z \ll \hat{u}_x, \hat{u}_y$ ). It is further assumed that the velocity field  $\mathbf{u}$  in both cases is of the same order (even though it has perpendicular directions), in order to be able to compare the vertical and horizontal convection effects.

The length scales are selected as  $L_z = H_5 - H_1$  in the vertical direction; radially it moves between  $L_1$  and  $L_2$ , and, if the food is of liquid-type, between 0 and  $L_1$ , and therefore the radial length scale is taken to be the maximum between  $L_1$  and  $L_2 - L_1$  or, for the sake of simplicity,  $L_r = L_2$ .

In the vertical case, equation (8) can be written as

$$\frac{\partial \hat{T}}{\partial \hat{t}} - \frac{\bar{k}\tau}{\bar{\rho}\bar{C}_p} \left( \frac{1}{L_r^2} \left( \frac{\partial^2 \hat{T}}{\partial \hat{x}^2} + \frac{\partial^2 \hat{T}}{\partial \hat{y}^2} \right) + \frac{1}{L_z^2} \frac{\partial^2 \hat{T}}{\partial \hat{z}^2} \right) + \frac{\tau U}{L_z} \hat{u}_z \frac{\partial \hat{T}}{\partial \hat{z}} = \frac{\alpha\gamma\tau}{\bar{\rho}\bar{C}_p t_p} \hat{T}, \quad (9)$$

where the terms with  $\hat{u}_x$  and  $\hat{u}_y$  have been neglected because of the previous assumption  $\hat{u}_z \gg \hat{u}_x, \hat{u}_y$ . Thus, in this case there is a convective coefficient  $c_v = \frac{\tau U}{L_z}$ .

In the horizontal case, equation (8) results in

$$\begin{aligned} \frac{\partial \hat{T}}{\partial \hat{t}} - \frac{\bar{k}\tau}{\bar{\rho}\bar{C}_p} \left( \frac{1}{L_r^2} \left( \frac{\partial^2 \hat{T}}{\partial \hat{x}^2} + \frac{\partial^2 \hat{T}}{\partial \hat{y}^2} \right) + \frac{1}{L_z^2} \frac{\partial^2 \hat{T}}{\partial \hat{z}^2} \right) \\ + \frac{\tau U}{L_r} \left( \hat{u}_x \frac{\partial \hat{T}}{\partial \hat{x}} + \hat{u}_y \frac{\partial \hat{T}}{\partial \hat{y}} \right) = \frac{\alpha\gamma\tau}{\bar{\rho}\bar{C}_p t_p} \hat{T}, \quad (10) \end{aligned}$$

where now the  $\hat{u}_z$  term has been neglected due to the previous assumption  $\hat{u}_z \ll \hat{u}_x, \hat{u}_y$ . Thus, in this case there is a convective coefficient  $c_h = \frac{\tau U}{L_r}$ . It can be seen that the relation between  $c_v$  and  $c_h$  is  $c_v = c_h \left( \frac{L_r}{L_z} \right)$ .

Looking at the dimensions of the HP system,  $H_5 = 0.472$  m and  $H_1 = 0.222$  m, so  $L_z = 0.25$  m, and  $L_2 = 0.05$  m, which makes  $L_r = 0.05$  m. Using these values,  $c_v = \frac{c_h}{5}$ , so the convection effects are about 5 times larger in the horizontal case than in the vertical one. If  $L_r$  was  $L_2 - L_1$ , instead of  $L_2$ , then this difference would increase from 5 to nearly 10 times.

Also, it has to be pointed out that in the horizontal case, the convective currents reach the food sample sooner than in the vertical case, as they move mainly in the radial direction (see Figures 6a, 6b, 10a, 10b), which is smaller than the vertical direction. A fluid particle that is closer to the cold wall (especially to the top wall - this is, in the horizontal case) will in general take less time to reach the food sample than the same particle in the vertical case. This is why the systems placed horizontally cool the sample much faster than the vertically oriented ones, resulting in lower temperatures throughout the process.

### 3. Numerical tests

#### 3.1. Dimensions of the HP pilot unit

For the numerical tests a similar size of the pilot unit (ACB GEC Alsthom, Nantes, France) that was used in Otero et al. (2007) is considered. The dimensions of the system are given in Table 1. The numerical tests are computed in cylindrical coordinates for the 2D model, assuming cylindrical coordinates and Cartesian coordinates for the 3D-model. The Finite Element Method (FEM) solver COMSOL Multiphysics 3.5a was used to compute the solutions. More details of the computations will be given in Section 4.

#### 3.2. Process conditions

##### 3.2.1. Process $P_1$ : Moderate temperature and pressure

The following HP processes with different initial temperature and pressure curve (see process  $P_2$  in Infante et al. (2009)) are considered: The initial temperature is  $T_{0_1} = 40^\circ\text{C}$  in the whole domain  $\Omega$  and the pressure is linearly increased during the first 183 seconds until it reaches  $P_{\max_1} = 360$  MPa. Thus, the pressure generated by the equipment satisfies  $P(0) = 0$  and

$$\frac{dP_1}{dt}(t) = \begin{cases} \frac{360}{183} \cdot 10^6 \text{ Pa s}^{-1}, & 0 < t \leq 183, \\ 0 \text{ Pa s}^{-1}, & t > 183. \end{cases} \quad (11)$$

##### 3.2.2. Process $P_2$ : High temperature and pressure

Also considered is a HP process with higher temperatures and pressures (to achieve typical thermal pasteurisation values and to reflect pressures of current cold HPP pasteurisation processes): The initial temperature is  $T_{0_2} = 65^\circ\text{C}$  in the whole domain  $\Omega$  and the pressure is linearly increased during

the first 200 seconds until it reaches  $P_{\max_2} = 600$  MPa. Thus, the pressure generated by the equipment satisfies  $P(0) = 0$  and

$$\frac{dP_2}{dt}(t) = \begin{cases} \frac{600}{200} \cdot 10^6 \text{ Pa s}^{-1}, & 0 < t \leq 200, \\ 0 \text{ Pa s}^{-1}, & t > 200. \end{cases} \quad (12)$$

### 3.3. Thermo-physical parameters

For the sake of simplicity, the physical parameters of the pressurising medium and the liquid-type food are assumed to be those of water. The mean values in the relevant range of temperature and pressure for each of the processes are given in Table 1. The thermo physical properties of the steel and rubber cap of the sample holder are assumed to be constant, and obviously the same for both processes, and their values are also in Table 1. The reference temperature  $T_r$  for both processes is taken to be equal to the initial temperature; and the environment temperature,  $T_{\text{env}}$ , is taken as 19.3°C (which is a reasonable room temperature).

### 3.4. Computational methods

The partial differential equations describing the model were solved with the Finite Element Method (FEM) using COMSOL Multiphysics™ (COMSOL AB, Stockholm, Sweden) a commercial software package. For each geometry the mesh was different, using tetrahedral elements for the 3D models and triangular elements for the 2D models. The computations were carried out on different workstations and the solving time for all cases was different (obviously for the 3D models it was much longer than the 2D models). Details can be seen in Table 2. It has to be noted that even though the number of elements for the 3D vertical case was slightly higher than for the 3D horizontal case, the computational solving time was much longer for the horizontal model. This is due to the fact that the horizontal flow moves faster than the vertical one, and thus the Navier-Stokes equations are more complex to solve and therefore, computational demand is significantly greater.

## 4. Numerical results and discussion

### 4.1. Comparison between 2D axis-symmetric and 3D vertical models

Firstly, we compared the results of the 2D axis-symmetric and 3D vertical models, which we expect to be nearly identical. The comparison was

Table 1: Typical parameter values for both processes. The food and the pressurising fluid properties are those of water in the adequate range of temperature and pressure. Data obtained from Cleland & Earle (1995); Infante et al. (2009); Otero et al. (2006). [Notation and units:  $\bar{\rho}_1 = \bar{\rho}_{F_1} = \bar{\rho}_{P_1}$ ,  $\bar{\rho}_2 = \bar{\rho}_{F_2} = \bar{\rho}_{P_2}$  ( $\text{kg m}^{-3}$ );  $\bar{C}_{p_1} = \bar{C}_{p_{F_1}} = \bar{C}_{p_{P_1}}$ ,  $\bar{C}_{p_2} = \bar{C}_{p_{F_2}} = \bar{C}_{p_{P_2}}$  ( $\text{J kg}^{-1} \text{K}^{-1}$ );  $\bar{k}_1 = \bar{k}_{F_1} = \bar{k}_{P_1}$ ,  $\bar{k}_2 = \bar{k}_{F_2} = \bar{k}_{P_2}$  ( $\text{W m}^{-1} \text{K}^{-1}$ );  $\bar{\alpha}_1 = \bar{\alpha}_{F_1} = \bar{\alpha}_{P_1}$ ,  $\bar{\alpha}_2 = \bar{\alpha}_{F_2} = \bar{\alpha}_{P_2}$  ( $\text{K}^{-1}$ );  $\eta$  ( $\text{Pa s}$ );  $h$  ( $\text{W m}^{-2} \text{K}^{-1}$ );  $T_1 = T_{0_1} = T_{r_1}$ ,  $T_2 = T_{0_2}, T_{r_2}$  ( $^{\circ}\text{C}$ );  $P$  ( $\text{MPa}$ ); Dimensions of HP system (m); Time (s)]

$\bar{\rho}_1$	973.856	$\bar{\rho}_2$	1068.2	$\rho_S$	7833	$\rho_C$	1110
$\bar{C}_{p_1}$	4686.65	$\bar{C}_{p_2}$	3900.9	$C_{p_S}$	465	$C_{p_C}$	1884
$\bar{k}_1$	0.649	$\bar{k}_2$	0.7848	$k_S$	55	$k_C$	0.173
$\bar{\alpha}_1$	$4.574 \cdot 10^{-4}$	$\bar{\alpha}_2$	$5.03 \cdot 10^{-4}$	$\alpha_S$	0	$\alpha_C$	0
$\bar{\eta}_1$	$8.069 \cdot 10^{-4}$	$\bar{\eta}_2$	$4.36 \cdot 10^{-4}$	$\eta_S$	0	$\eta_C$	0
$T_{\text{env}}$	19.3	$T_1$	40	$T_2$	65		
$P_{\text{max}_1}$	360	$P_{\text{max}_2}$	600	$h$	28		
$L_1$	0.02	$L_2$	0.05	$L$	0.09	$H_1$	0.222
$H_2$	0.254	$H_3$	0.404	$H_4$	0.439	$H_5$	0.472
$H$	0.654	$t_{p_1}$	183	$t_{p_2}$	200	$t_f$	900

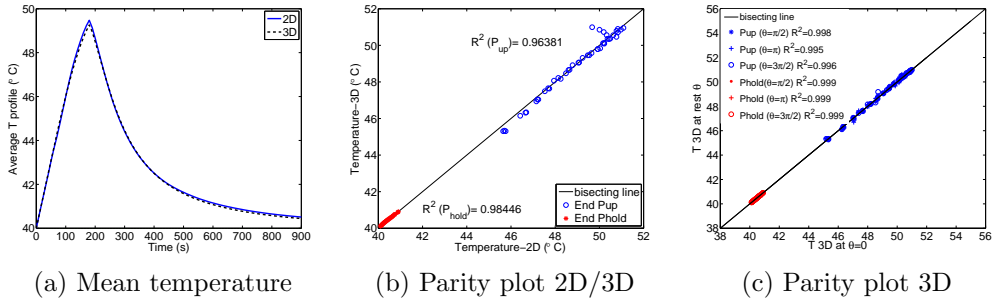


Figure 3: Different plots for 2D and 3D vertical models; Process 1.

performed in 45 locations (covering an axis-symmetric plane with a 3 x 15 matrix) at three different radial coordinates (symmetry axis, 9 mm distance from symmetry axis and 18mm distance from symmetry axis) and fifteen different heights (10 mm steps, from 6 mm above the sample holder bottom to 4 mm below the sample holder top) of the food sample region. This

Table 2: Characteristics of the computational methods for the different models.

Model	Comsol Version	Number of mesh elements	Workstation characteristics	Comp. time (s)
2D V	3.5a	1526	2 dual-core proc (2.33 GHz) 4 GB RAM 64bit OS W2003	220
3D V	3.5a	73843	2 dual-core proc (2.33 GHz) 4 GB RAM 64bit OS W2003	144000
3D H	4.2a	66306	4 dual-core proc (3.40 GHz) 8 GB RAM 64bit OS W7	330949

comparison with the same points was repeated for different planes in the 3D model (at angles  $\theta = 0, \pi/2, \pi, 3\pi/2$ ). The 3D temperature variable is taken as the average of the temperature over these different planes. A comparison of the 2D and 3D models shows that the model outcome for the temperature was indeed very similar. Figures 3a and 4a show the average temperature over time of the 2D axis-symmetric and 3D vertical model for processes  $P_1$  and  $P_2$ , respectively, with very good agreement. Figures 3b and 4b show the parity plots for the predicted temperature from the 2D axis-symmetric and 3D vertical model for processes  $P_1$  and  $P_2$ , respectively. The coefficient of determination  $R^2$  were greater than 0.9, for both processes, at the end of pressurisation ( $P_{up}$ ) and at the end of the process ( $P_{hold}$ ). Figures 3c and 4c show the parity plot for the predicted temperatures of the 3D model along the different planes (at angles  $\theta = 0, \pi/2, \pi, 3\pi/2$ ), for processes  $P_1$  and  $P_2$ , respectively. The coefficients of determination  $R^2$  were greater than 0.99, for both process, at the end of pressurisation ( $P_{up}$ ) and at the end of the process ( $P_{hold}$ ).

It has to be pointed out that the 2D axis-symmetric solution could have been even closer to the 3D vertical solution if the 3D mesh had been further refined. However, given that the objective in this paper was to compare the 3D vertical to the 3D horizontal model, and taking into account the long computational time the 3D models took (see Table 2), it was considered unnecessary to further refine the mesh to improve the 2D axis-symmetric to 3D vertical solution similarity.

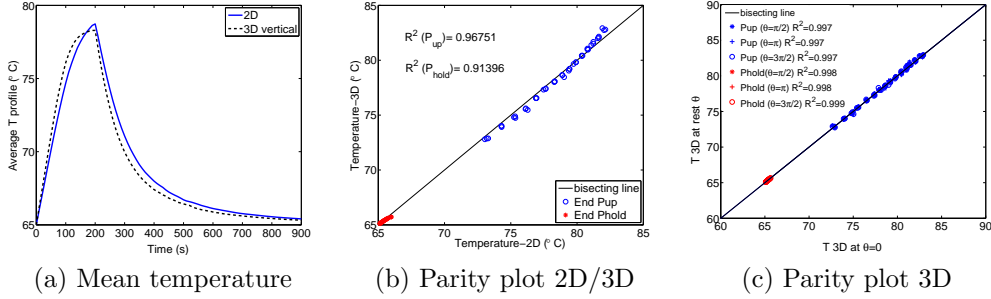


Figure 4: Different plots for 2D and 3D vertical models; Process 2.

#### 4.2. Comparison between 3D vertical and 3D horizontal models

The next step was to compare the 3D vertical and 3D horizontal models. Obviously, the results of these models will no longer be the same. It is expected that the temperatures will be different due to the differences in the flow. To compare the results from the different models, a MATLAB routine was developed to extract temperature data from the models in COMSOL, in several configurations:

- Over the entire liquid food domain with a  $1 \text{ mm}^3$  resolution (i.e. looking at the same points for both cases), which will give an idea of the overall difference in temperature performance.
- On the central radial slice of the liquid food domain for both orientations, to help visualise the spatial differences radially.
- For further information on spatial differences 5 radial slices are selected (and points on them at  $1 \text{ mm}^2$  resolution) along the height in the vertical case (starting from the bottom of the food sample holder and separated by  $0.0375 \text{ m}$ ), and the same slices along the length in the horizontal case. The central radial slice of the previous point coincides with the third slice here. This will give an idea of the temperature behaviour radially but also at different heights.
- Along the central axis of the food sample domain, which will help to illustrate the temperature differences with height at the same radial point.

For all of these data sets the averaged temperature over time is plotted with standard deviations at ten time steps for both models, and for both processes  $P_1$  and  $P_2$ . Tables 3 and 4 show the temperature mean values (measure of performance) and standard deviation values (measure of uniformity) at the end of pressurisation ( $P_{\text{up}}$ ) and end of the process ( $P_{\text{hold}}$ ), for all of these sets of data, for the 3D vertical and horizontal models, and for process  $P_1$  and  $P_2$ , respectively

To illustrate the differences in temperature distribution inside the vessel and also the qualitative difference in the flow distribution, slice plots of the temperature and velocity field inside the food sample and pressurising media at the end of the pressurisation ( $P_{\text{up}}$ ) and also at the end of the process ( $P_{\text{hold}}$ ), separately for the vertical and horizontal cases are included.

#### 4.2.1. Process $P_1$ : Moderate temperature and pressure

Figures 5 and 6 show the slice plots for process  $P_1$  at the end of  $P_{\text{up}}$  and  $P_{\text{hold}}$  for the vertical and horizontal model, respectively. As can be seen, the distribution for the vertical model is almost uniform in the radial direction but changes with height, whereas for the horizontal model the changes in length (equivalent to height for the vertical case) are insignificant, but there are differences in the radial direction. Focusing on a certain length for the horizontal case it can be seen that the temperature at the top is higher than at the bottom, which is not the case in the vertical orientation (for the vertical orientation at a given height the temperature distribution inside the sample was more uniform). This can be explained by the fact that the cooling is coming from the boundary  $\Gamma_r$ , which in the horizontal case is at the top and bottom of the sample (as depicted in the slice plot), but when the system is rotated into a vertical position this boundary is at the left and right of the sample. In the vertical case, because the cooling was coming from the sides, it affected the flow uniformly, but now it is coming from above and below, and because of density differences the lower part is cooling faster than the top part.

For both models, at the end of  $P_{\text{up}}$ , the differences are more pronounced than at the end of  $P_{\text{hold}}$  due to the fact that the pressurisation induces a heat source, so the overall temperature is higher, and so are the temperature gradients. At the end of  $P_{\text{hold}}$  the sample has had enough time to cool down to the boundary temperature  $T_r$  almost everywhere and therefore the differences at different locations have reduced. Overall, the temperature of the vertical model is higher than that of the horizontal one, especially at the end of  $P_{\text{up}}$ .

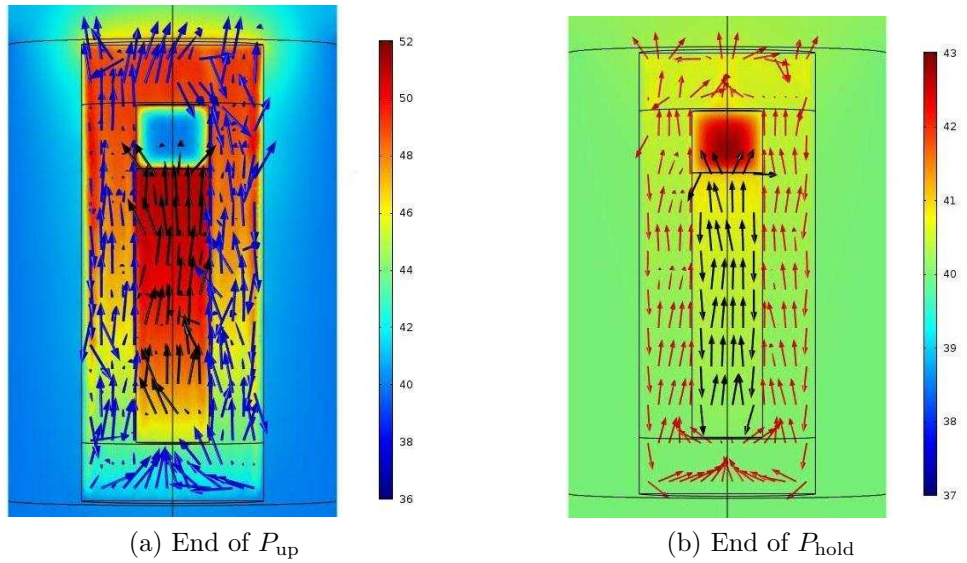


Figure 5: Slice plots of 3D vertical model; Process  $P_1$ .

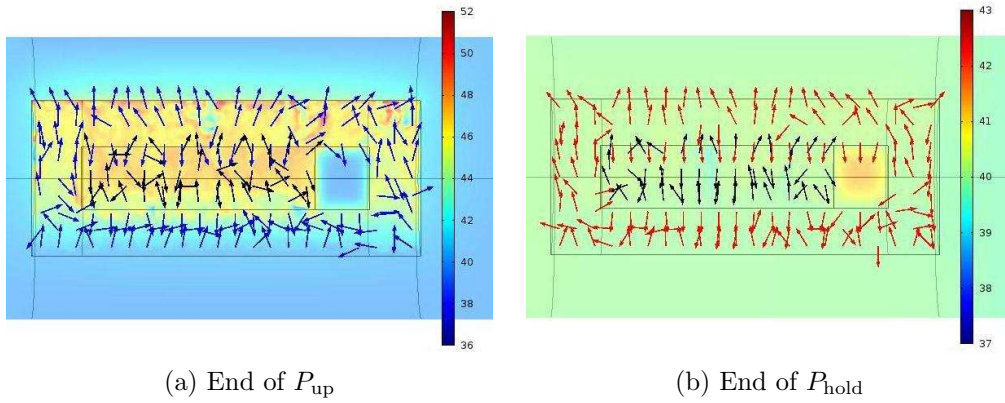


Figure 6: Slice plots of 3D horizontal model; Process  $P_1$ .

This is due to the fact that the flow is faster in the horizontal case, with more pronounced convective heat transfer, and therefore the sample temperature reaches the boundary temperature at  $\Gamma_r$  faster.

In Infante et al. (2009); Otero et al. (2007), the authors showed that the cooling is faster when convection is included in the model, compared to a conduction only model. So for faster flows this result also holds.

Looking at the qualitative distribution of the flow a difference between the

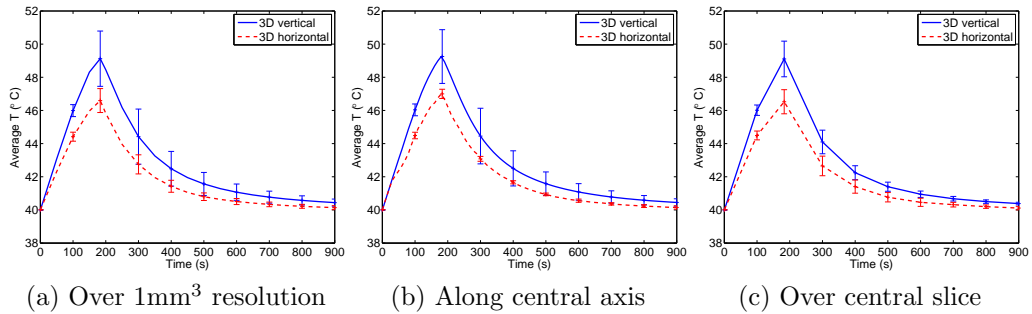


Figure 7: Averaged temperature evolution for different data sets; Process  $P_1$ .

vertical and horizontal model can be seen. For the vertical model, the flow moves longitudinally, whereas for the horizontal model the flow moves mainly radially. This is due to gravity and density differences and the location of the cooler boundary, as mentioned earlier. For the vertical model the cooler boundary is on the sides of the machine, therefore the flow moves downwards when it gets near to the outside of the machine and upwards near the centre of the sample, where temperatures are higher. For the horizontal model, the cooler boundary is now above and below the sample, resulting in a radial flow.

Figure 7 shows the averaged temperature evolution for the different data sets for process  $P_1$ , with error bars every 100 seconds. Figure 7a is the average over the  $1 \text{ mm}^3$  resolution matrix and as can be seen the temperature of the vertical model is higher than the horizontal, and so are the standard deviations. This is due to the fact that overall the differences in temperatures throughout the whole domain will be higher in the vertical than in the horizontal case, because the horizontal flow is faster and therefore temperature uniformity is reached sooner. Figure 7b is the average along the central axis of the food domain, and again the temperature is higher in the vertical than the horizontal model, and so are the standard deviations, which is to be expected as it shows that the temperature varies more with height in the vertical case than with length in the horizontal one. Figure 7c is the average over the central slice of the food domain. Again, the temperature in the vertical model is higher than the horizontal, but now the standard deviation bars are nearly equal for both processes. It was expected that they were greater in the horizontal case, due to the fact that at a given length the

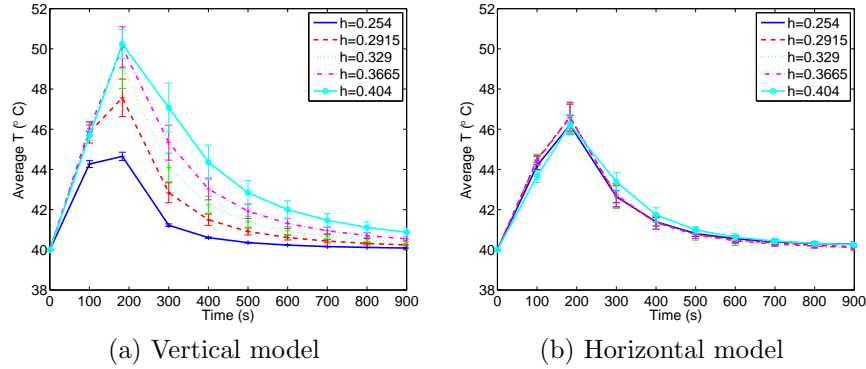


Figure 8: Averaged temperature over 5 radial slices; Process  $P_1$ .

temperature will vary more radially in the horizontal case than in the vertical one (where at a given height we expect uniform temperatures). However, for process  $P_1$  these variations are similar for both models. This is believed to be due to the fact that temperature variations in this process are quite small (between 40 and 52°C), and temperature uniformity is achieved more easily.

Figure 8 shows the averaged temperature evolution over the 5 different slices of the food domain, with error bars every 100 seconds, for process  $P_1$ . Figure 8a is for the vertical model and Figure 8b the horizontal. The temperature again is higher for the vertical model, and the differences of averaged temperature at different height are also higher in the vertical case, showing, again, that temperature varies more with height in the vertical case than with length in the horizontal case. As would be expected, the closer to the top of the food sample, the temperature of the vertical model is higher. In general, the standard deviations are also larger in the vertical case, which shows again the greater uniformity of the horizontal model in every direction, particularly in this process where the range of temperatures is not very wide.

Looking at Table 3 it can be seen that the horizontal model for process  $P_1$  is more uniform throughout most of the process and for all of the data sets. Closer to the end, i.e. near  $P_{\text{hold}}$ , both the horizontal and vertical models have similar mean values and show a similar extent of uniformity measurements, which agrees with what was seen in the plots (see Figures 7 and 8).

Table 3: Measure of performance and uniformity for 3D vertical and horizontal models (temperatures given in °C); Process  $P_1$ .

Process 1	3D Vertical		3D Horizontal	
	End $P_{up}$	End $P_{hold}$	End $P_{up}$	End $P_{hold}$
1 mm <sup>3</sup> mat	49.12 ± 1.67	40.44 ± 0.22	46.60 ± 0.72	40.14 ± 0.12
Slice 1	44.65 ± 0.21	40.09 ± 0.01	46.22 ± 0.49	40.27 ± 0.11
Slice 2	47.56 ± 0.93	40.24 ± 0.05	46.61 ± 0.74	40.15 ± 0.09
Slice 3	49.11 ± 1.08	40.38 ± 0.08	46.52 ± 0.73	40.11 ± 0.10
Slice 4	50.08 ± 1.02	40.54 ± 0.11	46.58 ± 0.67	40.16 ± 0.12
Slice 5	50.25 ± 0.72	40.88 ± 0.22	46.23 ± 0.50	40.25 ± 0.09
Central axis	49.26 ± 1.62	40.45 ± 0.22	47.00 ± 0.28	40.15 ± 0.10

#### 4.2.2. Process $P_2$ : Higher temperature and pressure

For process  $P_2$  the same analyses were performed. Figures 9 and 10 show the slice plots for temperature and flow distribution at the end of  $P_{up}$  and  $P_{hold}$ . The situation is very similar to the one described for the slice plots of process  $P_1$ . The one thing to highlight is that now the differences are qualitatively the same, but quantitatively higher, due to the fact that process  $P_2$  has a wider range of temperatures (between 65 and 85°C) than process  $P_1$  (between 40 and 52°C) because the maximum pressure reached is higher for process  $P_2$  (600 MPa) than for process  $P_1$  (360 MPa), and compression heating is also higher for higher initial temperatures (see, e.g., Knoerzer et al. (2010b)).

Figure 11 shows the averaged temperature evolution for the different data sets for process  $P_2$ , with error bars every 100 seconds. Figure 11a is the average over the 1 mm<sup>3</sup> resolution matrix and as can be seen, the temperature of the vertical is higher than in the horizontal model, and so are the standard deviations, i.e., same as for process  $P_1$ . Figure 11b is the average along the central axis of the food domain, and again the temperature predicted by the vertical model is higher than in the horizontal model, and so are the standard deviations. Figure 11c is the average over the central slice of the food domain. Again, the temperature in the vertical model is higher than in the horizontal model, but now the standard deviations are larger for the horizontal case, which is what was expected as mentioned previously. In this case this is more pronounced due to the fact that process  $P_2$  has a wider

range of temperatures than process  $P_1$  and therefore the temperature is not as uniform as before.

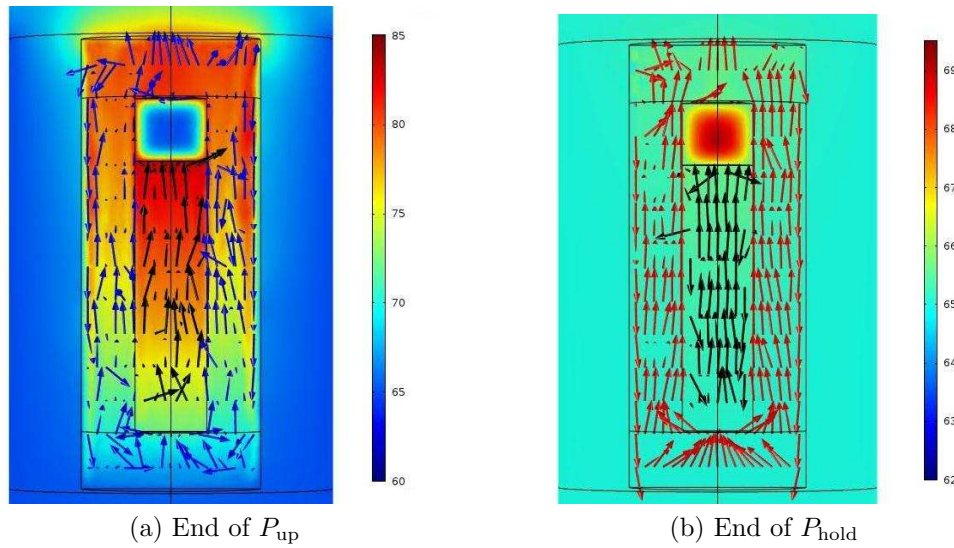


Figure 9: Slice plots 3D vertical model. Process  $P_2$

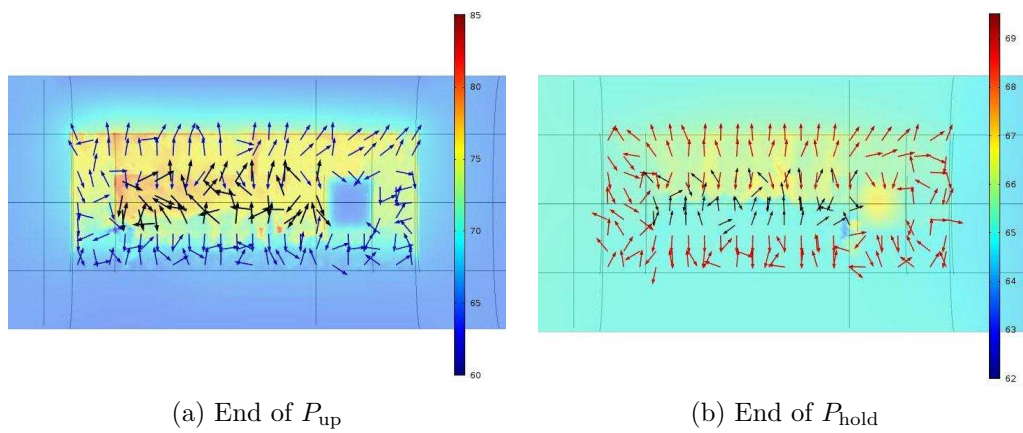


Figure 10: Slice plots 3D horizontal model. Process  $P_2$

Figure 12 shows the averaged temperature evolution for process  $P_2$ , over the 5 different slices of the food domain, with error bars every 100 seconds. Figures 12a and 12b are for the vertical and horizontal models respectively. The temperature again is higher for the vertical model, and the differences

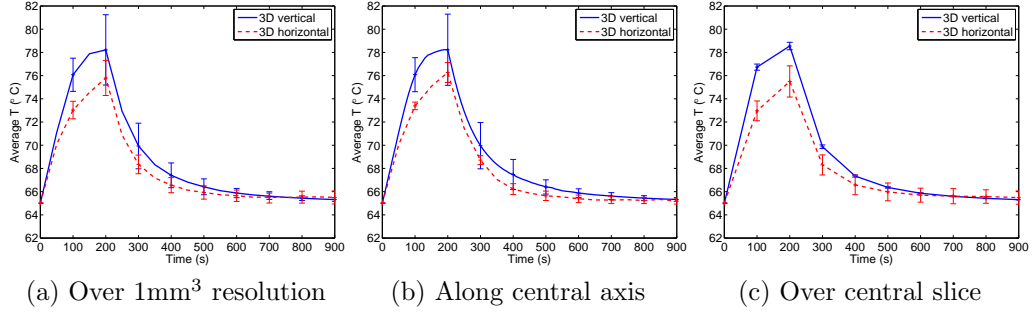


Figure 11: Averaged temperature evolution for different data sets. Process  $P_2$

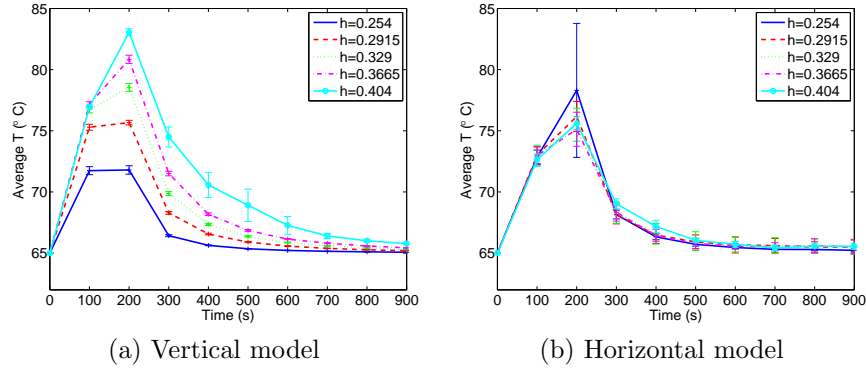


Figure 12: Averaged temperature over 5 radial slices; Process  $P_2$ .

of averaged temperature at different heights is also greater in the vertical case, showing, once again, that temperature varies more with height in the vertical case than with length in the horizontal case. However, now it can also be seen that the standard deviations are larger in the horizontal case. This makes sense since at a given height (or length) the radial differences are lower in the vertical configuration.

Table 4 shows that the horizontal model for process  $P_2$  is more uniform throughout most of the process and for all of the data sets, except for the slices. Closer to the end, i.e. near  $P_{\text{hold}}$ , both the horizontal and vertical models have similar mean values and uniformity measurements, which agrees with what was seen in the plots.

Table 4: Measure of performance and uniformity for 3D vertical and horizontal models (temperature measured in °C); Process  $P_2$ .

Process 2	3D Vertical		3D Horizontal	
	End $P_{up}$	End $P_{hold}$	End $P_{up}$	End $P_{hold}$
1 mm <sup>3</sup> mat	78.21 ± 3.03	65.32 ± 0.15	75.80 ± 1.15	65.50 ± 0.56
Slice 1	71.80 ± 0.35	65.07 ± 0.00	78.30 ± 5.48	65.23 ± 0.12
Slice 2	75.67 ± 0.19	65.20 ± 0.02	76.17 ± 1.23	65.52 ± 0.61
Slice 3	78.55 ± 0.32	65.31 ± 0.02	75.50 ± 1.34	65.49 ± 0.57
Slice 4	80.84 ± 0.33	65.43 ± 0.02	75.13 ± 1.39	65.51 ± 0.56
Slice 5	83.06 ± 0.28	65.77 ± 0.10	75.61 ± 0.53	65.55 ± 0.24
Central axis	78.19 ± 2.99	65.33 ± 0.16	76.27 ± 0.86	65.18 ± 0.22

## 5. Concluding remarks

Three dimensional vertical and horizontal models for High Pressure Thermal Processing were set up and compared. The results have shown that, as expected, the temperature performance and uniformity is different for the two geometries, which indicates that there is a need to further develop horizontal models, given that most industrial processes take place in horizontally oriented HP systems, and the published data to date are all for vertically oriented HP systems. For a liquid-type food (in this work water) and for a long and thin machine it was shown that the temperature in general is more uniform for the horizontal case, for the processes discussed. For the vertical model temperatures change along height, whilst for the horizontal model they change more radially.

## Acknowledgements

This work was carried out thanks to the financial support of the Spanish “Ministry of Economy and Competitiveness” under projects MTM2008-04621 and MTM2011-22658; the “Fundación Caja Madrid”; and the “Comunidad de Madrid” and “European Social Fund” through project S2009/PPQ-1551.

## Nomenclature

$\mathbf{A}_1, \mathbf{A}_2$	Pressure points
$C_p$	Specific heat capacity ( $\text{Jkg}^{-1}\text{K}^{-1}$ )
$\mathbf{g}$	Gravity constant vector ( $\text{ms}^{-2}$ )
$h$	Heat transfer ( $\text{Wm}^{-2}\text{K}^{-1}$ )
$H$	Domain height (m)
$k$	Conductivity ( $\text{Wm}^{-1}\text{K}^{-1}$ )
$L$	Domain width (m)
$L_r$	Radial length scale (m)
$L_z$	Vertical length scale (m)
$M$	Mass (kg)
$\mathbf{n}$	Outward normal unit vector (m)
$p$	Pressure in media (Pa)
$P$	Equipment Pressure (Pa)
$P_{\max}$	Maximum target pressure (Pa)
$r$	Radial coordinate (m)
$t$	Time (s)
$t_f$	Final time (s)
$t_{\text{up}}$	Pressurisation time (s)
$T$	Temperature (K)
$T_0$	Initial temperature (K)
$T_{\text{env}}$	Environment temperature (K)
$T_r$	Fixed temperature (K)
$\mathbf{u}$	Fluid velocity vector ( $\text{m s}^{-1}$ )
$u_x, u_y, u_z$	Components of $\mathbf{u}$
$U$	Velocity scale ( $\text{m s}^{-1}$ )
$V$	Volume ( $\text{m}^3$ )
$x, y, z$	Cartesian coordinates (m)

### Greek symbols

$\alpha$	Thermal expansion ( $\text{K}^{-1}$ )
$\Gamma$	Whole domain boundary
$\Gamma_p$	Boundary of $\Omega_p^*$
$\Gamma_r$	Fixed temperature boundary
$\Gamma_{\text{up}}$	Heat transfer boundary
$\eta$	Dynamic viscosity ( $\text{Pa s}$ )
$\theta$	Cylindrical angular coordinate
$\Theta$	Temperature scale (K)

$\rho$	Density ( $\text{kg m}^{-3}$ )
$\tau$	Time scale (s)
$\Omega$	Whole domain
$\Omega_C$	Cap of the sample holder domain
$\Omega_F$	Food sample domain
$\Omega_P$	Pressurising medium domain
$\Omega_S$	Steel vessel domain

### Abbreviations

CFD	Computational Fluid Dynamics
FEM	Finite Element Method
HP	High Pressure
HPP	High Pressure Processing
HPT	High Pressure Thermal
OS	Operation system
RAM	Random access memory
2D	Two-dimensional
3D	Three-dimensional

### Indices

*	Rotated domains
F	Food domain
hold	Pressure-hold solution
P	Pressurising fluid
up	Pressure-up solution

### Other symbols

$\nabla$	Gradient
$\nabla \cdot$	Divergence
$\nabla^2$	Laplacian

## References

- Cleland, A. C., & Earle, R. L. (1995). Assessment of freezing time prediction methods. *J. Food Sci.*, *49*, 1034–1042.
- Denys, S., Loey, A. M. V., & Hendrickx, M. E. (2000a). A modelling approach for evaluating process uniformity during batch high hydrostatic pressure processing: Combination of a numerical heat transfer model and enzyme inactivation kinetics. *Innovative Food Science and Emerging Technologies*, *1*, 5–19.
- Denys, S., Ludikhuyze, L. R., Loey, A. M. V., & Hendrickx, M. E. (2000b). Modeling conductive heat transfer and process uniformity during batch high-pressure processing of foods. *Biotechnol. Prog.*, *16*, 92–101.
- Ghani, A. G. A., & Farid, M. M. (2007). Numerical simulation of solid-liquid food mixture in a high pressure processing unit using computational fluid dynamics. *Journal of Food Engineering*, *80*, 13031–1042.
- Hartmann, C., & Delgado, A. (2002). Numerical simulation of convective and diffusive transport effects on a high - pressure - induced inactivation process. *Biotechnology and Bioengineering*, *79*, 94–104.
- Hartmann, C., & Delgado, A. (2003). Numerical simulation of thermal and fluid-dynamical transport effects on a high pressure induced inactivation. *High Pressure Research*, *23*, 67–70.
- Hartmann, C., Delgado, A., & Szymczyk, J. (2003). Convective and diffusive transport effects in a high pressure induced inactivation process of packed food. *Journal of Food Engineering*, *59*, 33–44.
- Hartmann, C., Schuhholz, J.-P., Kitsbun, P., Chapleau, N., Bail, A. L., & Delgado, A. (2004). Experimental and numerical analysis of the thermofluid-dynamics in a high-pressure autoclave. *Innovative Food Science and Emerging Technologies*, *5*, 399–411.
- Infante, J. A., Ivorra, B., Ramos, A. M., & Rey, J. M. (2009). On the modelling and simulation of high pressure processes and inactivation of enzymes in food engineering. *Math. Models Methods Appl. Sci.*, *19*, 2203–2229.

- Juliano, P., Knoerzer, K., Fryer, P., & Versteeg, C. (2008). *C. Botulinum* inactivation kinetics implemented in a computational model of a high pressure sterilization process. *Biotechnology Process*, *25*, 163–175.
- Knoerzer, K., Buckow, R., Juliano, P., Chapman, B., & Versteeg, C. (2010a). Carrier optimisation in a pilot-scale high pressure sterilisation plant – an iterative cfd approach. *Journal of Food Engineering*, *97*, 199–207.
- Knoerzer, K., Buckow, R., & Versteeg, C. (2010b). Adiabatic compression heating coefficients for high pressure processing – a study of some insulating polymer materials. *Journal of Food Engineering*, *98*, 110–119.
- Knoerzer, K., & Chapman, B. (2011). Effect of material properties and processing conditions on the prediction accuracy of a cfd model for simulating high pressure thermal (hpt) processing. *Journal of Food Engineering*, *104*, 404–413.
- Knoerzer, K., Juliano, P., Gladman, S., Versteeg, C., & Fryer, P. J. (2007). A computational model for temperature and sterility distributions in a pilot-scale high-pressure high-temperature process. *AIChE Journal*, *53*, 2996–3010.
- Kupper, A., Hauptmann, E. G., & Iqbal, M. (1969). Combined free and forced convection in a horizontal tube under uniform heat flux. *Solar Energy*, *12*, 439–446.
- Mujica-Paz, H., Valdez-Fragoso, A., Tonello-Samson, C., Welti-Chanes, J., & Torres, J. A. (2011). High-pressure processing technologies for the pasteurization and sterilization of foods. *Food Bioprocess Technol.*, *4*, 969–985.
- Oliver, D. R. (1962). The effect of natural convection on viscous-flow heat transfer in horizontal tubes. *Chemical Engineering Science*, *17*, 335–350.
- Otero, L., Ousegui, A., Guignon, B., Bail, A. L., & Sanz, P. D. (2006). Evaluation of the thermophysical properties of tylose gel under pressure in the phase change domain. *Food Hydrocolloids*, *20*, 449–460.
- Otero, L., Ramos, A. M., de Elvira, C., & Sanz, P. D. (2007). A model to design high pressure processes towards a uniform temperature distribution. *J. Food Engng*, *78*, 1463–1470.

**PREPUBLICACIONES DEL DEPARTAMENTO  
DE MATEMÁTICA APLICADA**  
UNIVERSIDAD COMPLUTENSE DE MADRID  
MA-UCM 2012

1. ON THE CAHN-HILLIARD EQUATION IN  $H^1(\mathbb{R}^N)$ , J. Cholewa and A. Rodríguez Bernal
2. GENERALIZED ENTHALPY MODEL OF A HIGH PRESSURE SHIFT FREEZING PROCESS, N. A. S. Smith, S. S. L. Peppin and A. M. Ramos
3. 2D AND 3D MODELING AND OPTIMIZATION FOR THE DESIGN OF A FAST HYDRODYNAMIC FOCUSING MICROFLUIDIC MIXER, B. Ivorra, J. L. Redondo, J. G. Santiago, P.M. Ortigosa and A. M. Ramos
4. SMOOTHING AND PERTURBATION FOR SOME FOURTH ORDER LINEAR PARABOLIC EQUATIONS IN  $\mathbb{R}^N$ , C. Quesada and A. Rodríguez-Bernal
5. NONLINEAR BALANCE AND ASYMPTOTIC BEHAVIOR OF SUPERCRITICAL REACTION-DIFFUSION EQUATIONS WITH NONLINEAR BOUNDARY CONDITIONS, A. Rodríguez-Bernal and A. Vidal-López
6. NAVIGATION IN TIME-EVOLVING ENVIRONMENTS BASED ON COMPACT INTERNAL REPRESENTATION: EXPERIMENTAL MODEL, J. A. Villacorta-Atienza and V.A. Makarov
7. ARBITRAGE CONDITIONS WITH NO SHORT SELLING, G. E. Oleaga
8. THEORY OF INTERMITTENCY APPLIED TO CLASSICAL PATHOLOGICAL CASES, E. del Rio, S. Elaskar, and V. A. Makarov
9. ANALYSIS AND SIMPLIFICATION OF A MATHEMATICAL MODEL FOR HIGH-PRESSURE FOOD PROCESSES, N. A. S. Smith, S. L. Mitchell and A. M. Ramos
10. THE INFLUENCE OF SOURCES TERMS ON THE BOUNDARY BEHAVIOR OF THE LARGE SOLUTIONS OF QUASILINEAR ELLIPTIC EQUATIONS. THE POWER LIKE CASE, S. Alarcón, G. Díaz and J.M.Rey
11. SUSTAINED INCREASE OF SPONTANEOUS INPUT AND SPIKE TRANSFER IN THE CA3-CA1 PATHWAY FOLLOWING LONG TERM POTENTIATION IN VIVO, O. Herreras, V. Makarov and A. Fernández-Ruiz
12. ELLIPTIC EQUATIONS IN WEIGHTED BESOV SPACES ON ASYMPTOTICALLY FLAT RIEMANNIAN MANIFOLDS, U. Brauer and L. Karp
13. A NUMERICAL METHOD TO SOLVE A DUOPOLISTIC DIFFERENTIAL GAME IN A CLOSED-LOOP EQUILIBRIUM, J. H. de la Cruz, B.Ivorra and A. M. Ramos
14. EVALUATION OF THE RISK OF CLASSICAL SWINE FEVER SPREAD IN BULGARIA BY USING THE EPIDEMIOLOGICAL MODEL BE-FAST, B. Martínez-López. B.Ivorra, A. M. Ramos, E. Fernández, T. Alexandrov and J.M. Sánchez-Vizcaíno
15. WAVE-PROCESSING OF LONG-SCALE INFORMATION IN NEURONAL CHAINS, J. A. Villacorta-Atienza and V. A. Makarov
16. A NOTE ON THE EXISTENCE OF GLOBAL SOLUTIONS FOR REACTION-DIFFUSION EQUATIONS WITH ALMOST-MONOTONIC NONLINEARITIES, A. Rodríguez-Bernal and A. Vidal-López

**PREPUBLICACIONES DEL DEPARTAMENTO  
DE MATEMÁTICA APLICADA**  
UNIVERSIDAD COMPLUTENSE DE MADRID  
MA-UCM 2013

1. THIN DOMAINS WITH DOUBLY OSCILLATORY BOUNDARY , J.M. Arrieta and M Villanueva-Pesqueira
2. ESTIMATES ON THE DISTANCE OF INERTIAL MANIFOLDS, J.M. Arrieta and E. Santamaría
3. A PRIORI BOUNDS FOR POSITIVE SOLUTIONS OF SUBCRITICAL ELLIPTIC EQUATIONS, A. Castro and R. Pardo
4. EVALUATION OF THE DIFFERENCES OF PROCESS VARIABLES IN VERTICAL AND HORIZONTAL CONFIGURATIONS OF HIGH PRESSURE THERMAL (HPT) PROCESSING SYSTEMS THROUGH NUMERICAL MODELLING, N. A. S. Smith, K. Knoerzer and A. M. Ramos